Synthesis and Characterization of Efficient ZnO/g-C₃N₄ Nanocomposites Photocatalyst for Photocatalytic Degradation of Methylene Blue

Renathung C. Ngullie [1], Saleh O. Alaswad [2], Kandasamy Bhuvaneswari [3], Paramasivam Shanmugam [1,*], Thangavelu Pazhanivel [3] and Prabhakarn Arunachalam [4,*]

[1] Department of Chemistry, St. Joseph University, Dimapur, Nagaland 797115, India; ngullierena@gmail.com
[2] Nuclear Science Research Institute (NSRI), King Abdulaziz City for Science and Technology (KACST), P.O. Box 6086, Riyadh 11442, Saudi Arabia; salaswad@kacst.edu.sa
[3] Smart Materials Interface Laboratory, Department of Physics, Periyar University, Salem-636 011, India; bhuviphy11@gmail.com (K.B.); pazhanit@gmail.com (T.P.)
[4] Electrochemistry Science Research Chair (ESRC), Chemistry Department, College of Science, King Saud University, Riyadh 11451, Saudi Arabia
* Correspondence: shanmugachem@gmail.com (P.S.); parunachalam@ksu.edu.sa (P.A.); Tel.: +91-9884284640 (P.S.); +966-507564123 (P.A.)

check for updates

Abstract: We examine the photocatalytic activity (PCA) of ZnO/graphitic carbon nitride g-C₃N₄ (g-CN) composite material for methylene blue (MB) degradation under visible-light irradiation (VLI). The polymeric g-CN materials were fabricated by the pyrolysis of urea and thiourea. More importantly, ZnO/g-CN nanostructured composites were fabricated by adding the different mounts (60, 65, 70, and 75 wt.%) of g-CN into ZnO via the simple hydrothermal process. Among fabricated composites, the 75% ZnO/g-CN nanocomposites displayed a superior PCA for MB degradation, which were ~three-fold an enhancement over the pure ZnO nanoparticles. The fabricated materials have been evaluated by X-ray diffraction (XRD), UV-Vis, Fourier transform infrared (FT-IR) spectroscopy, and electron microscopy. More importantly, the photodegradation of MB could get 98% in ZnO/g-CN could be credited to efficient separation of photo-induced charge carriers between ZnO and g-CN. Also, the recycling efficiency of the as-prepared composites was studied for multiple cycles, which shows that the photocatalysts are stable and suitable to carry out photocatalytic degradation in the logistic mode. Additionally, the probable photocatalytic mechanism has also discussed. The synthetic procedure of ZnO/g-CN based materials can be used in numerous fields such as environmental and in energy storage applications.

Keywords: ZnO; carbon nitride; ZnO/carbon nitride nanocomposites; hydrothermal; photocatalysts

1. Introduction

In the modern world, consumption of non-renewable fossil fuels by the growing human population is resulting in a rapid depletion of fuels and ecological pollution at a frightening rate [1,2]. Currently, water pollution is highlighted as a vital concern for human beings, as it is frequently being influenced by numerous toxic pollutants such as textiles, cosmetics, food, and paint industries [3,4]. In this regard, there are several techniques available for handling polluted water, visible-light-based photocatalysis is considered to be a green approach and has fascinated globally owing to its inexhaustible solar energy [5–7]. Typically, photocatalytic features are generally ruled by its inherent physicochemical natures of materials, including its band-gap position, surface area, pore size, and morphological structures [8–11] Until now, the existing photocatalytic semiconductors such as the metal oxides and

sulfides, oxynitrides, polymers, and organic metal complexes have been demonstrated to possess effective photocatalytic features. Among these, semiconductor metal oxides, such as ZnO, TiO_2, Cu_2O, CuO, NiO, $BiVO_4$, WO_3, and ZnO, have the efficiency to maximize the absorption of incident photons [12–14]. More importantly, wider band-gap semiconductor materials such as TiO_2, ZnO, and $SrTiO_3$ are already recognized as effective photocatalytic materials due to its great redox potential of photoinduced charge carriers [15,16]. In recent years, n-type ZnO semiconductors are preferred, due to its low cost, eco-friendly, simple synthetic procedure, and wide bandgap with comparison to TiO_2. Particularly, the photocatalytic performance of ZnO was comparatively better than TiO_2 in few reports. For instance, Sakthivel et al., also reported visible-light assisted photodegradation of azo dye: competition of photocatalytic efficiency [17]. However, ZnO or other single metal-based materials mostly suffered from photocorrosion and have average performance. On this regard, few scientific efforts are now dedicated to finding suitable approaches for decreasing the recombination rate of charge carriers working under VLI [18,19].

In recent years, various reports are carried out to promote the PCA employing conventional several supporting candidates which can haste an efficient separation of photoinduced charge carriers, namely semiconductors, graphene, CNT, and other carbonaceous materials. In particular, Vadivel et al. reported the $BiPO_4$/multi-walled carbon nanotubes (MWCNTs) composites for the photocatalyst and supercapacitor applications [20]. Similarly, the fabrication of graphene and MWCNTs supported materials are economically expensive and produce toxicity during functionalization [21]. To solve the problems, the researcher introduced polymeric g-CN materials incorporates with semiconductor materials. More importantly, g-CN is used to improve the electron-hole pair recombination rate, stable, inexpensive, proper band position, low-cost characteristic, easily separable, unique properties, and also examined as the visible-light active materials [22–25]. The CN photocatalyst materials possessing conjugated electronic alignment with the band-gap of nearly 2.7 eV, holds greater thermal, chemical, electro-optical properties [26,27]. During the past decades, Wang et al. demonstrated the polymeric g-CN photocatalytic materials for a visible-light-assisted water-splitting reaction [28]. The metal-free g-CN is restricted by lower photocatalytic activity due to fast charge recombination. Afterward, Pragati et al., studied the degradation of methylene blue (MB) using ZnO/g-CN as a photocatalyst, urea carbon source [29].

The metal-free g-CN can be fabricated by the direct pyrolysis of different organic precursors. The commercially accessible urea and thiourea were recognized as green organic precursors for the fabrication of g-CN. It was evidenced that the usage of urea and thiourea might evolve CO_2, H_2S, NH_3, and H_2O vapor during the pyrolysis process [30], which can be employed as a bubble soft template. Also, g-CN with the enriched surface area was fabricated by annealing both precursors of urea and thiourea, which were recrystallized in ethanol. More importantly, Zhang et al. revealed that the fabricated g-CN with the mixture of thiourea and urea exhibits the greater specific surface area and enhanced PCA compared to g-CN derivatives from the mixture of urea and thiourea [31]. Also, numerous research efforts have been found for homogeneous carbon sources like urea, melamine, formaldehyde resin and thioureas derived graphitic carbon and are incorporated with semiconductor nanoparticle [32–34]. Numerous g-CN-based heterojunctions photocatalysts have been developed by coupling g-CN with different inorganic photocatalysts [35–43]. For instance, effective combinations of catalysts comprise heterojunctions of graphene/g-CN, Au/g-CN, TiO_2/g-CN, MoS_2/g-CN, TaON/g-CN, ZnO/g-CN, Bi_2WO_6/g-CN, CdS/g-CN, WO_3/g-CN, and BiOBr/g-CN [35–43].

The PCA of ZnO is restricted owing to its wider bandgap and photoinduced charge carriers are easy to recombine. Also, the incorporation of various metal ions onto ZnO photocatalysts can efficiently enhance PCA [44–48]. Recently, doped ZnO-based photocatalysts have been demonstrated improved photocatalytic features for MB degradation [49]. Similarly, it is also revealed that the stability and PCA of ZnO can be promoted by loading with carbonaceous materials. Recently, Raghavan et al. fabricated a reduced graphene oxide (rGO)/TiO_2/ZnO system via a two-step solvothermal process [50]. Tien et al. demonstrated a hybrid photocatalyst composed of rGO and ZnO spheres by an easy and

rapid microwave-assisted solvothermal reaction [51]. The formation of heterojunctions between ZnO and g-CN has the potential to develop efficient materials for photocatalytic applications. In this regard, it is imperious to synthesize a different variety of carbon sources to fabricate polymeric g-CN catalysts by a simple and cost-effective method. Hence, in this work, we have fabricated g-CN-based materials derived from the mixture of urea/thiourea.

Herein, ZnO/g-CN nanocomposites were fabricated by a simple and cost-efficient deposition-precipitation method, and its catalytic activity was investigated through photodegradation of MB. The graphitic CN was prepared by urea and thiourea mixture using the pyrolysis method. More importantly, ZnO/CN nanocomposite shows excellent activity in as than its corresponding pristine ZnO and g-CN. Because of the type-II band position of ZnO and g-CN, the interface between g-CN and ZnO benefits the rapid transport of photoinduced charge carriers, thus influenced ZnO/CN to be efficient photocatalysts. More importantly, photostability and reusability of fabricated composites investigation were also completed to identify the reactive species and explore the stability and reusability of composite materials for long time use. Lastly, a feasible photodegradation mechanism of MB above synthesized ZnO/g-CN nanocomposites has also been proposed.

2. Experimental Details

2.1. Materials

Zinc Sulfate (99.5%), sodium hydroxide (98%), and ethanol (99%) were purchased from SRL chemicals (Mumbai, India). Urea (99.5%) and thiourea (99%) were purchased from Nice Chemicals (P) Ltd. (Ernakulam, India), MB dye was purchased from Loba Chemie (P) Ltd. (Mumbai, India).

2.2. Preparation of g-CN/Zn Ophotocatalyst

The g-CN was fabricated via a pyrolysis method in which 6 g of urea and 6 g of thiourea were taken in two different 100 mL beakers and dissolved in 20 mL of deionized water [4]. Afterward, the prepared solution of urea and thiourea were mixed and then dried in an oven at around 80 °C. After which the dried reaction mixture is transferred into a crucible and heated at 550 °C for 5 h with the heating rate of 15 °C/min. Subsequently, the attained g-CN metal-free heterojunction photocatalysts were obtained. To prepare g-CN/ZnO nanocomposites were fabricated by a simple hydrothermal process. Typically, 50 mL of $ZnSO_4 \cdot 7H_2O$ (0.05 moles, 0.72 g) solution were taken in a 100-mL beaker, and then an appropriate quantity of g-CN was dispersed using a sonicator. To prepare different nanocomposites, the amount of ZnO contents in g-CN/ZnO composites were varied from 60 to 75 wt.%. Further, 50 mL of NaOH (1.0 M, 2 g) solution was introduced under magnetic stirring. Subsequently, the whole reaction mixture was moved to stainless-steel autoclave and kept in oven 180 °C for 12 h. After the hydrothermal process, the attained precipitate was then filtered and washed about 3–4 times and then dried around 60 °C for 24 h. The similar procedure used to prepare other composites viz., g-CN/ZnO 60, 65, 70, and 75 wt.% of ZnO materials. According to this method, bare-ZnO was also prepared through the same hydrothermal process.

2.3. Materials Characterization

The phase purity and crystalline nature of g-CN/ZnO nanocomposites were collected and analyzed by using XRD techniques (Rigaku ULTIMA 1V IR-Technology service Pvt. Ltd., Tokyo, Japan). The surface functional group and introduction of the ZnO onto the surface of g-CN were studied using FT-IR on a Cary 630 FT-IR Agilent Technologies India Pvt. Ltd., United States. The surface morphology and size of the g-CN, ZnO and its composites were used to study field emission scanning electron microscope (FE-SEM) Carl Zeiss: Sigma, Germany. A high-resolution transmission electron microscope (HR-TEM) was performed on a JEOL: JEM2100 PLUS, Tokyo, Japan operating at 200 kV. The photocatalytic performance of the g-CN, ZnO, and its composites were studied using UV-Vis spectroscopy (Shimadzu, Model UV-3600, Kyoto, Japan).

2.4. Photocatalytic Study

PCA of the fabricated photocatalytic materials was examined by the degradation of MB solution under VLI. The photocatalyst solution was prepared by the addition of 0.1 g of catalyst into a 100 mL MB (50 mg/L) solution irradiation. Initially, a sorption balance has been achieved between the MB solution and catalyst after stirring 60 min without VLI. After that, the prepared photocatalyst solutions were treated with VLI with a 500 W Xe Lamp, where the UV-light ($\lambda < 420$) had been prevented by a cut off filter. At a particular time interval, 0.2 mL of solution was withdrawn and then centrifuged to eliminate the catalyst particles. The absorption concentrations of the MB dye solution were spectrophotometrically observed by assessing the absorbance of solutions at 664 nm during the degradation process at numerous time intervals. The absorbance maximum at $\lambda = 664$ nm was employed to estimate the concentration of the MB dye solution. The photodegradation of dye is conveyed by C/C_0; Where C_0 is the residual concentration of MB, and C is the primary concentration of the MB.

3. Results and Discussion

XRD analysis was used to assess the phase purity and crystalline nature of the fabricated samples. Figure 1a shows the powder XRD patterns of the prepared bare-ZnO, g-CN, and a series of g-CN/ZnO nanocomposites. As seen from Figure 1a, observed peaks at 31.8°, 34.43°, 36.27°, 47.57°, 56.67°, 62.93°, 67.99°, and 69.20° and the corresponding diffraction plans from (100), (002), (101), (102), (110), (103), (112), and (201) planes clearly indicated that hexagonal wurtzite crystal phase of ZnO (JCPDS card # 89-0510) [12]. Also, the powdered XRD patterns of ZnO particles display the peak of $Zn(OH)_2$ (Figure 1a). Particularly, the pure g-CN sample has two distinct peaks at $2\theta = 13.34°$ and $27.38°$ which can be related to (100) and (002) diffraction planes (JCPDS No. 87-1526) [22]. Also, the peak positioned at 13.34° related to the in-plane packing motif (100) peak of tristriazine units. In particular, the distance is estimated to be 0.675 nm, which is agreed to the hole-to-hole distance in the nitride pores. Simultaneously, another intense peak of 27.38° is related to C–N aromatic stacking units with a distance of 0.324 nm, attributing to the (002) plane of the interlayer stacking of the conjugated aromatic system. In this regard, the sharp and intense diffraction peaks of both g-CN and ZnO evidenced their crystallinity nature. In fabricated composites, all the series of g-CN/ZnO nanocomposites shows the identical distinctive diffraction peaks with the bare-ZnO. With the ZnO incorporation over the g-CN, the ZnO crystalline peaks appeared at g-CN/ZnO composites. There is no impurity found in the g-CN/ZnO composites, thus confirmed the successfully prepared high purity of g-CN and g-CN/ZnO nanocomposites. Further, the average particle size of the ZnO particles was used to calculate Scherrer's equation, the obtained particle size was 40 ± 2 nm. These results revealed that the ZnO fabricated onto g-CN with the chemical bonding of Zn–N was successfully achieved via condensation reactions.

Figure 1b shows the FT-IR spectra of ZnO, g-CN, and a series of g-CN/ZnO photocatalysts with different ZnO contents. FT-IR spectra of g-CN showed the following characteristic bands; C–N stretching vibration mode at the wavenumber of 1628 cm^{-1} and the aromatic C–N stretching modes are observed at 1230, 1398, and 1543 cm^{-1} [52]. Also, the band witnessed at 802 cm^{-1} is credited to out-of-plane bending modes of C–N heterocycles [53]. More importantly, the FT-IR spectrum of independent-ZnO, the peak located at 591 cm^{-1} was assigned to the stretching vibration of Zn–O [53]. Further, a broad absorption peak positioned at 3500 cm^{-1} was owing to the existence of water molecules [54]. More importantly, Figure 1b also displays the FT-IR spectra of a series of ZnO/g-CN composite materials, the observed peaks are identical to those of peaks of g-CN are observed in the composite. However, with the increase in the percentage of ZnO (60% to 75%), the peak intensity also increased. Also, it is evidenced that the obtained peaks correspond to the g-CN and ZnO are witnessed in the g-CN/ZnO composite materials. All results have shown that the fabricated materials were nanocomposite rather than a physical combination of two distinct phases ZnO and g-CN.
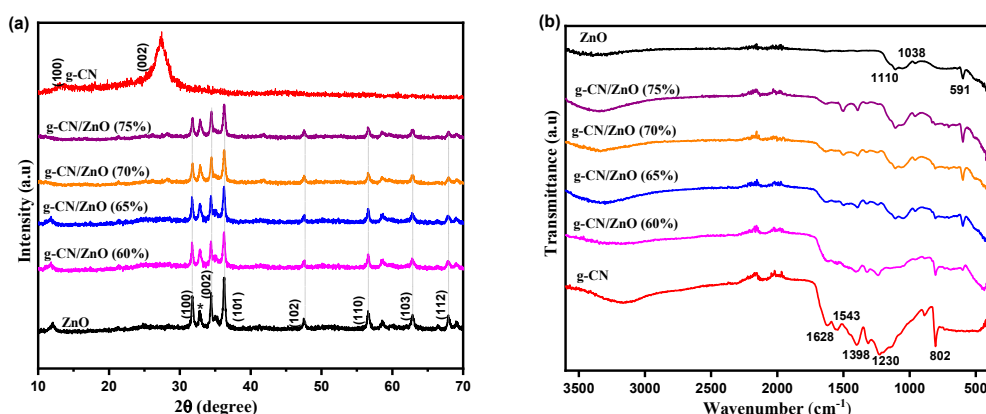
Figure 1. (**a**) XRD pattern of g-CN, ZnO, g-CN/ZnO (60%), g-CN/ZnO (65%), g-CN/ZnO (70%), and g-CN/ZnO (75%). The Powdered XRD pattern for composite corresponds to pure ZnO (wurtzite); (**b**) and its corresponding Fourier transform infrared (FT-IR) spectra of fabricated materials.

The surface morphology and microstructure of the g-CN, ZnO and g-CN/ZnO (75%) composites were inspected through FE-SEM as presented in Figure 2. Figure 2a shows the FE-SEM images of g-CN which is composed of nanosheets sheets like structures and fluffier. Also, hydrothermally fabricated ZnO particles are obtained with an irregularly aggregated spherical particle (Figure 2b). Interestingly, the surface morphology of fabricated g-CN/ZnO (75%) composites (Figure 2c,d) contains both spherical ZnO particles and nanosheet morphologies, which were homogeneously dispersed. Thus the fabricated binary nanocomposites materials are expected to play a vital role in determining its photocatalytic performances.
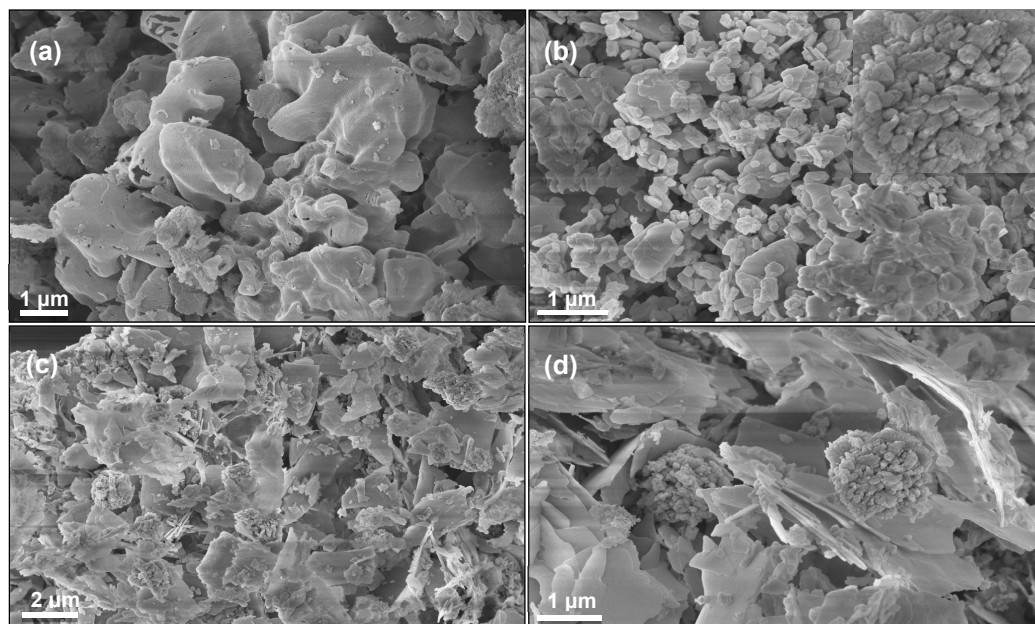

Figure 2. Field emission scanning electron microscope (FE-SEM) image of: (**a**) g-CN, (**b**) bare-ZnO, and (**c**,**d**) g-CN/ZnO (75%) composite materials prepared using a hydrothermal process.

To further assess the morphological features of fabricated composites, the HR-TEM measurements were carried out and are depicted in Figure 3. HR-TEM images of g-CN/ZnO (75%) composite as seen in Figure 3a,b, clearly observed the darker particles of ZnO over the thin layer sheets of g-CN, which is consistent with FE-SEM analysis. Furthermore, HR-TEM of a composite at higher magnifications to observe more number of fringe patterns of ZnO particles over g-CN sheets (Figure 3c,d). The observed

interplanar distance (d) of 0.252 nm is observed to have matched with the lattice fringe spacing of the (101) ZnO hexagonal wurtzite phase, which also reveals the interface between the hexagonal ZnO and g-CN sheets [12]. Inset of Figure 3d reveals the respective selected area electron diffraction (SAED) pattern of g-CN. These morphological investigations evidenced the interface between g-CN nanosheets and ZnO particles in the composites and are appropriate candidate materials to enhance the charge-separation and thereby enhancement of the PCA.
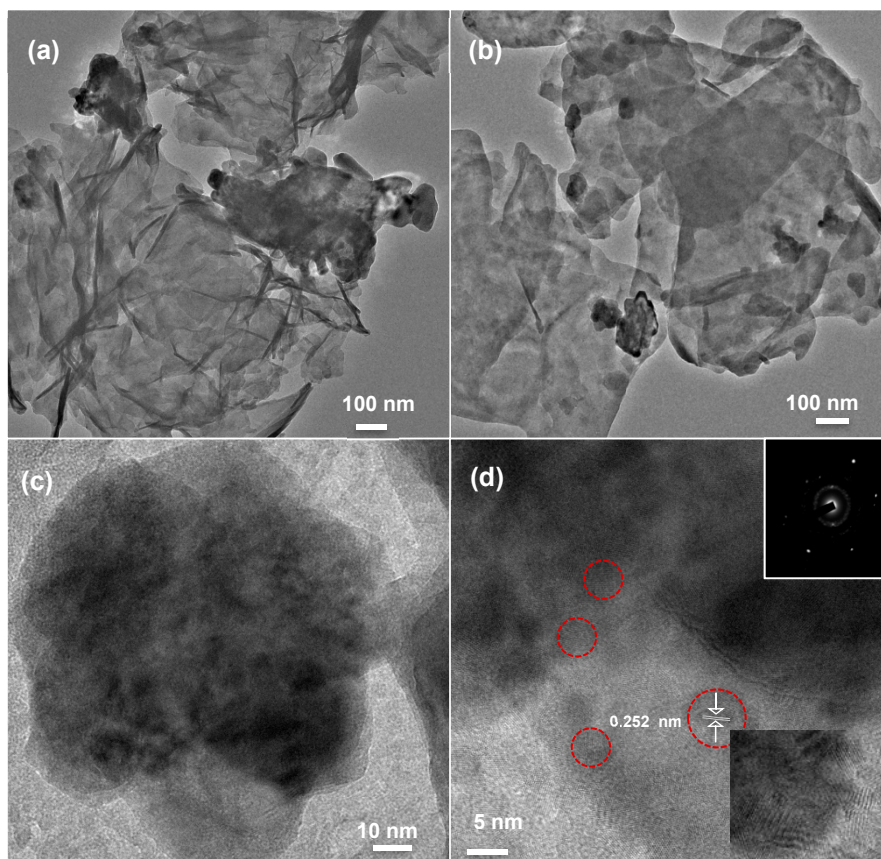

Figure 3. High-resolution transmission electron microscope (HR-TEM) images of: (**a**,**b**) g-CN/ZnO (75%) (low magnification), (**c**,**d**) g-CN/ZnO (75%) (high magnification), and the inset shows the diffraction pattern of CN/ZnO (75%).

3.1. Photocatalytic Activity

The photocatalytic MB dye degradation performances of ZnO and g-CN/ZnO photocatalyst were studied under VLI. In a typical process, the maximum absorption concentration MB dye peak at 664 nm was taken to investigate the catalytic degradation of MB dye. Particularly, the time-dependent absorption spectra of MB with differently prepared photocatalysts were displayed in Figure 4. The maximum absorption intensity MB dye was slowly decreased in the presence of pristine ZnO with the illumination of VLI. The observed result clearly shows the low degradation efficiency of pristine ZnO nanoparticles (Figure 4a). Moreover, after the addition of g-CN into the ZnO nanoparticles, the catalytic activity was gradually increased which means the g-CN nanosheets are influenced toward the enhanced PCA. Interestingly, the photodegradation efficiency of the g-CN/ZnO (75%) photocatalysts was considerably greater than that of pristine ZnO and other combinations of g-CN/ZnO. Amongst all the as-prepared samples, g-CN/ZnO (75%) exhibited improved catalytic activity because of the enhanced visible-light absorption and suppressed recombination rate in comparison with bare ZnO photocatalyst or g-CN. Similarly, g-CN provided more active surface and strong absorption capacity to MB dye molecules. Furthermore, the layered nanosheets structure of g-CN favored the

photogenerated electron-hole transfer from g-CN to ZnO. It is a significant factor in photocatalytic activities of g-CN/ZnO (75%) nanocomposites as photocatalysts.
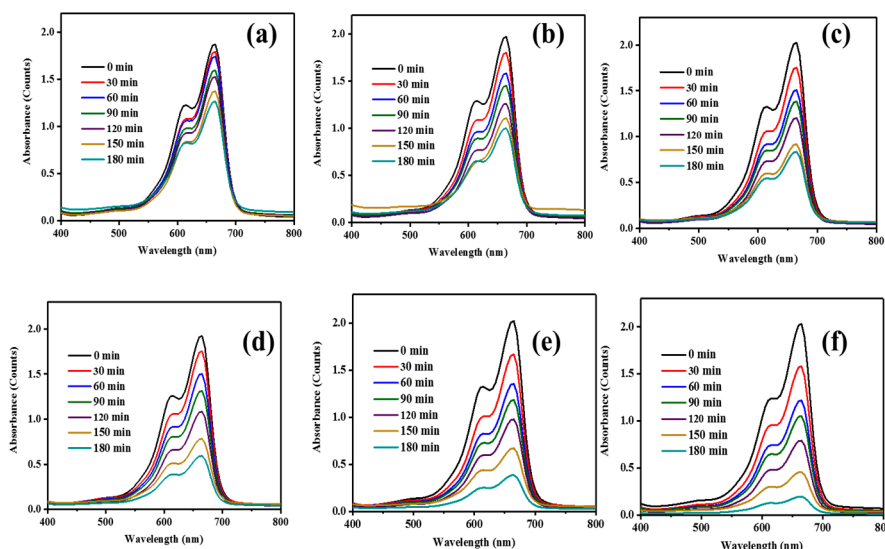

Figure 4. UV-Vis absorbance spectra of visible-light degradation of methylene blue (MB) dye in the presence of (**a**) bare-ZnO, (**b**) undoped g-CN, (**c**) g-CN/ZnO (60%), (**d**) g-CN/ZnO (65%), (**e**) g-CN/ZnO (70%), and (**f**) g-CN/ZnO (75%).

Figure 5 reveals the photodegradation of MB over bare-ZnO, undoped g-CN, and a series of g-CN/ZnO composites. The blank analysis was performed without a catalyst to determine the stability of MB under illumination conditions and the results indicated that the MB was stable under illumination. Figure 5 shows the kinetic plot of (C_0/C_t) vs. irradiation time (min) to examine the degradation of MB dye in the presence of as-prepared catalysts.
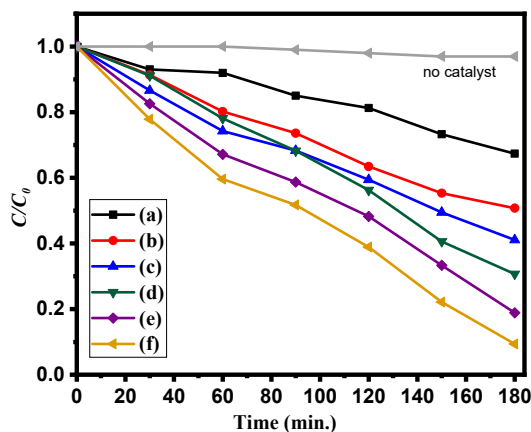

Figure 5. Photodegradation of MB dye over the presence of: (a) bare-ZnO, (b) undoped g-CN, (c) g-CN/ZnO (60%), (d) g-CN/ZnO (65%), (e) g-CN/ZnO (70%), and (f) g-CN/ZnO (75%).

Further, to understand the reaction kinetics of the MB degradation catalyzed by fabricated catalysts, the experimental data were fitted by a first-order kinetic model as shown by following Equation (1):

$$\ln(C_0/C) = kt \tag{1}$$

where C_0 and C are the initial and concentration of MB at a certain time interval and *k* is the rate constant. Figure 6 shows the linear fitting kinetic plot for the degradation of MB for fabricated catalysts.

The observed results clearly show that the prepared catalyst obeyed the pseudo-first-order kinetics. The calculated rate constants (K_{app}), agreeing with correlation coefficients (R^2), and maximal dye degradation in the presence of pristine and g-CN/ZnO nanocomposites are given Table 1. The estimated *k* values for the bare ZnO, bare g-CN, g-CN/ZnO (60%), g-CN/ZnO (70%), and g-CN/ZnO (75%) are found to be 0.0021, 0.0038, 0.0047, 0.009, and 0.0128 min^{-1}, correspondingly. Also, it is demonstrated that g-CN/ZnO (75%) composite has a greater rate constant which was ~6-folds superior to the bare ZnO. The existence of more reacting species, larger surface area, and enriched acting sites are improving the PCA. More importantly, the observed rate constant value also larger than that obtained for Fe-doped ZnO as reported by Isai et al [55] and larger with that observed for boron-doped g-CN-based composite [56].
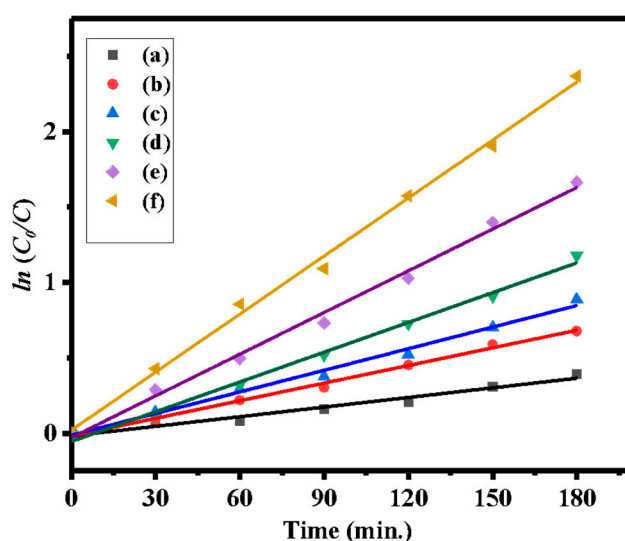

Figure 6. Pseudo-first-order kinetic plots of: (a) bare ZnO, (b) bare g-CN, (c) g-CN/ZnO (60%), (d) g-CN/ZnO(65%), (e) g-CN/ZnO (70%), and (f) g-CN/ZnO (75%).

Table 1. Data obtained from a pseudo-first-order kinetic linear fit of as-prepared catalyst.

Sample	Bare ZnO	Bare g-CN	g-CN/ZnO (60%)	g-CN/ZnO (65%)	g-CN/ZnO (70%)	g-CN/ZnO (75%)
Intercept	−0.0155 ± 0.018	−0.0159 ± 0.012	−0.010 ± 0.023	−0.0532 ± 0.026	−0.027 ± 0.03	0.0217 ± 0.038
Rate Constant	0.0021 ± 0.00017	0.00389 ± 0.000119	0.00477 ± 0.00021	0.00658 ± 0.000242	0.00922 ± 0.0003295	0.01283 ± 0.0003542
R-Square	0.96877	0.99535	0.99045	0.99328	0.99365	0.9962

Figure 7 shows the photodegradation efficiency of as-prepared nanocomposite samples in comparison with bare samples. The bare ZnO, bare g-CN, g-CN/ZnO (60%), g-CN/ZnO (65%), g-CN/ZnO (70%), and g-CN/ZnO (75%) materials are found to degrade around 26%, 45%, 60%, 69%, 80%, and 91% the MB solution under 120 min of irradiation. These results evidenced that with an increase in the amount of ZnO into the g-CN the PCA also gradually increased. The observed degradation result confirms that the g-C$_3$N$_4$ prominently improve the PCA.
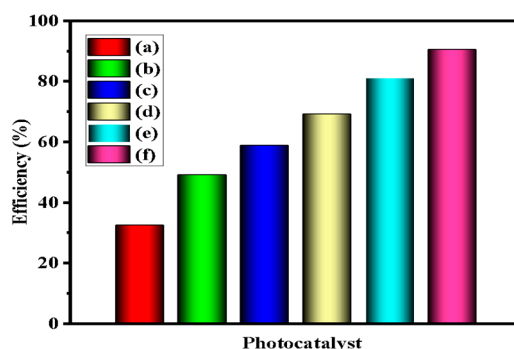
Figure 7. MB dye degradation efficiency of as-prepared catalysts: (a) bare-ZnO, (b) undoped g-CN, (c) g-CN/ZnO (60%), (d) g-CN/ZnO(65%), (e) g-CN/ZnO (70%), and (f) g-CN/ZnO (75%).

3.2. Reactive Species Studies

To know the role of active species in the MB dye degradation activity, radical trapping tests were performed, as displayed in Figure 8. The close inter-phase contact coupling of g-CN and ZnO particles in g-CN/ZnO must play a major part in improving PCA [39,57]. In general, the close coupling of ZnO/g-Cn nanoparticles results in promoting the electron transfer between interfaces and hindering the recombination of photoinduced charge carriers [58]. Usually, during the photocatalysis process, hydroxyl, holes, and superoxide radicals are the promising reactive species for the degradation of organic pollutants [59]. Herein, isopropyl alcohol (IPA), triethanolamine (TEOA), and p-benzoquinone (BQ) which are engaged as the scavengers for hydroxyl, holes, and superoxide radicals, correspondingly [12]. In a scavenger free reaction, the MB dye maximum degradation efficiency was observed up to 90.64% in 180 min irradiation for g-CN/ZnO (75%). So the g-CN/ZnO (75%) samples were selected to investigate the radical trapping study. After the introduction of radical trapping agents into the photocatalytic reaction, the degradation efficiency was decreased particularly, the observed efficiency was 90.6, 42.1, 76.3, and 62.9 percentages for without scavenger, TEOA, BQ, and IPA, respectively. This investigation confirmed that hole played a major role in the photocatalytic MB degradation compared to other radicals which means that after the addition of TEOA into the reaction nearly 60% of the efficiency was hindered. Hence, these results show that MB degradation mainly is governed by photogenerated holes.
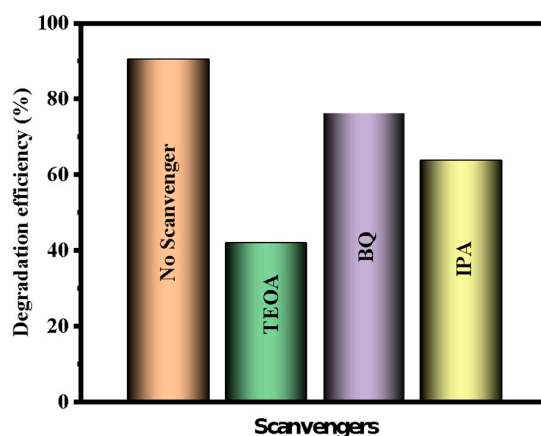

Figure 8. Influence of radical scavengers for the photodegradation of MB on g-CN/ZnO (75%) nanocomposite under illumination conditions.

3.3. Reusability Studies

The stability of the synthesized catalyst materials was examined by recycling the photocatalysts for the photocatalytic degradation of MB dye. Each cycle, a fresh MB dye solution was used for the next photocatalytic test. The catalyst particles were collected by centrifuged and washed, with distilled

water then reused. As shown in Figure 9, no major reduction was observed in the efficiency after four consecutive cycles, as a result, the g-CN/ZnO (75%) photocatalysts were photostable.
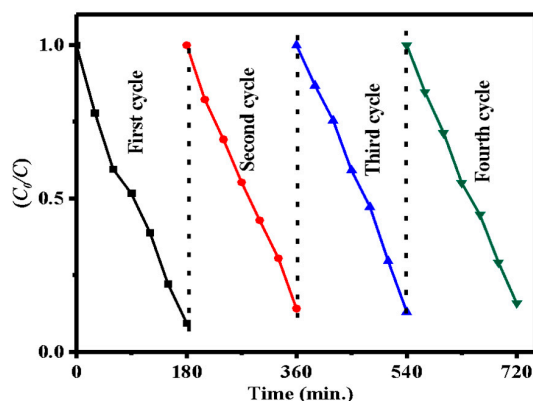

Figure 9. Recycling stability studies for the catalytic degradation of MB dye on g-CN/ZnO (75%) composites under illumination.

3.4. Mechanism

The apparent charge-transfer mechanism for MB degradation over g-CN/ZnO system was presented in Figure 10. As it is known that, the pure ZnO cannot be excited by visible light irradiation, the photodegradation of MB can mainly be attributed to the photogenerated hole oxidation and photoreduction process. On comparing pure g-CN, the g-CN/ZnO photocatalysts exhibited remarkable enhancement for degrading MB under visible light. The CB and VB edge potentials of as-synthesized pristine ZnO and g-CN were acquired from Butler–Ginley method [60,61]. The CB and VB edge potentials of the g-CN were calculated to be −1.12 and +1.57 eV, while the CB and VB edge position of ZnO are −0.26 and +2.83 eV, respectively. The appropriate band positions of g-CN and ZnO endorse the creation of the heterojunction and thereby improvement in PCA. According to the proposed mechanism, both ZnO and g-CN are expected to be photoinduced to create carriers. Under VLI conditions, since the CB potential of g-CN is more negative than that of ZnO, the photogenerated electrons on g-CN particle surfaces transfer easily to ZnO through the well-developed interface [62]. So the excited electron on g-CN could directly inject into the CB of ZnO. The electron-hole separations are also driven by the internal reassembly rebuilt electric fields in the two semiconductors. This decreases the strength of electron-hole recombination and leads to large numbers of electrons on the ZnO surface and holes on the g-CN surface, respectively, thus promoting the photocatalytic reactions to degradation MB.
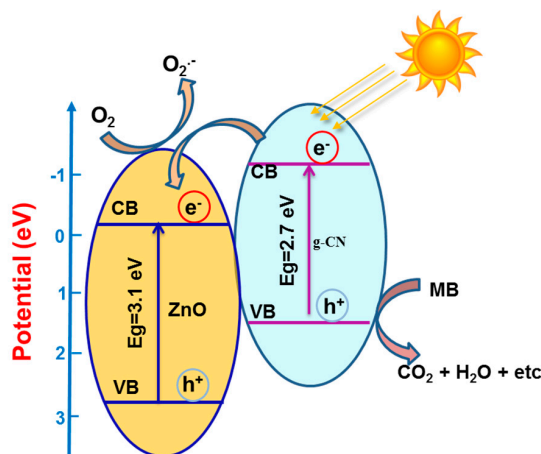

Figure 10. Proposed Z-scheme mechanism for enhanced photocatalytic features of MB over fabricated g-CN/ZnO composite under visible-light irradiation (VLI).

4. Conclusions

In conclusion, we adopted a facile hydrothermal approach to produce new g-CN/ZnO composites for photocatalytic decomposition of MB under VLI. The various compositions of g-CN/ZnO composites in the range of ZnO from 60% to 75% were prepared. The structural analysis of the g-CN/ZnO composite was studied using XRD, FT-IR, SEM, and TEM techniques. The g-CN/ZnO composites exhibited higher PCA and an easy recycling process, but ZnO easily suffered photocorrosion. The main reason could be suggested that the porous nature of g-CN can effectively separate photoinduced charge carries and diminish the photocorrosion of ZnO and thereby extraordinarily enhance visible-light PCA for the photodegradation of pollutants. The obtained results reveal that the g-CN/ZnO (75%) composites can effectively degrade 98% of MB dye within 180 min under UV light which is greatly superior to that of ZnO and g-CN. More importantly, the PCA of g-CN/ZnO under VLI was increased six times for the degradation of MB in comparison to bare ZnO. In the photodegradation of MB by g-CN/ZnO composites, photoinduced holes are the major species. Besides, benefiting from the graphitic carbon nitride excellent supporting materials, green synthetic, cost-effective of precursors, the obtained flexible heterojunctions g-CN/ZnO composites provide very fascinating prospects and may be stretched to the applications such as adsorbents, electrochemical materials, and support for sensors.

Author Contributions: R.C.N. and P.S performed the experiments and wrote the manuscript. S.O.A., T.P., and K.B. provided suggestions and assistance in experimental design. P.S. and P.A. assisted in experimental work and manuscript editing. All authors have read and agreed to the published version of the manuscript.

Conflicts of Interest: The authors declare no conflict of interest.

References

1. Gaya, U.I.; Abdullah, A.H. Heterogeneous photocatalytic degradation of organic contaminants over titanium dioxide: A review of fundamentals, progress and problems. *J. Photochem. Photobiol. C Photochem. Rev.* **2008**, *9*, 1–12. [CrossRef]

2. Guo, F.; Cai, Y.; Guan, W.; Huang, H.; Liu, Y. Graphite carbon nitride/ZnIn$_2$S$_4$ heterojunction photocatalyst with enhanced photocatalytic performance for degradation of tetracycline under visible light irradiation. *J. Phys. Chem. Solids* **2017**, *110*, 370–378. [CrossRef]

3. Bora, L.V.; Mewada, R.K. Visible/solar light active photocatalysts for organic effluent treatment: Fundamentals, mechanisms and parametric review. *Renew. Sustain. Energy Rev.* **2017**, *76*, 1393–1421. [CrossRef]

4. Xu, Q.; Feng, J.; Li, L.; Xiao, Q.; Wang, J. Hollow ZnFe$_2$O$_4$/TiO$_2$ composites: High-performance and recyclable visible-light photocatalyst. *J. Alloys Compd.* **2015**, *641*, 110–118. [CrossRef]

5. Yu, C.; Cao, F.; Li, G.; Wei, R.; Yu, J.C.-M.; Jin, R.; Fan, Q.; Wang, C. Novel noble metal (Rh, Pd, Pt)/BiOX(Cl, Br, I) composite photocatalysts with enhanced photocatalytic performance in dye degradation. *Sep. Purif. Technol.* **2013**, *120*, 110–122. [CrossRef]

6. Yang, L.; Duan, W.; Jiang, H.; Luo, S.; Luo, Y. Mesoporous TiO$_2$@Ag$_3$PO$_4$ photocatalyst with high adsorbility and enhanced photocatalytic activity under visible light. *Mater. Res. Bull.* **2015**, *70*, 129–136. [CrossRef]

7. Nazari, M.; Golestani-Fard, F.; Bayati, R.; Eftekhari-Yekta, B. Enhanced photocatalytic activity in anodized WO$_3$-loaded TiO$_2$ nanotubes. *Superlattices Microstruct.* **2015**, *80*, 91–101. [CrossRef]

8. Dong, F.; Zhao, Z.; Xiong, T.; Ni, Z.; Zhang, W.; Sun, Y.; Ho, W.K. In situ construction of g-C$_3$N$_4$/g-C$_3$N$_4$ metal-free heterojunction for enhanced visible-light photocatalysis. *ACS Appl. Mater. Interfaces* **2013**, *5*, 11392–11401. [CrossRef]

9. Xiang, Q.; Yu, J.; Jaroniec, M. Graphene-based semiconductor photocatalysts. *Chem. Soc. Rev.* **2012**, *41*, 782–796. [CrossRef]

10. Tong, H.; Ouyang, S.; Bi, Y.; Umezawa, N.; Oshikiri, M.; Ye, J. Nano-photocatalytic materials: Possibilities and challenges. *Adv. Mater.* **2012**, *24*, 229–251. [CrossRef]

11. Di Paola, A.; García-López, E.; Marcì, G.; Palmisano, L. A survey of photocatalytic materials for environmental remediation. *J. Hazard. Mater.* **2012**, *211*, 3–29. [CrossRef]

12. Priya, A.; Arumugam, M.; Arunachalam, P.; Al-Mayouf, A.M.; Madhavan, J.; Theerthagiri, J.; Choi, M.Y. Fabrication of visible-light active BiFeWO$_6$/ZnO nanocomposites with enhanced photocatalytic activity. *Colloids Surf. A Physicochem. Eng. Asp.* **2020**, *586*, 124294.

13. Theerthagiri, J.; Salla, S.; Senthil, R.A.; Nithyadharseni, P.; Madankumar, A.; Arunachalam, P.; Maiyalagan, T.; Kim, H.-S.; Jayaraman, T.; Kim, H.S.; et al. A review on ZnO nanostructured materials: Energy, environmental and biological applications. *Nanotechnology* **2019**, *30*, 392001. [CrossRef]

14. Malathi, A.; Madhavan, J.; Ashokkumar, M.; Arunachalam, P. A review on BiVO$_4$ photocatalyst: Activity enhancement methods for solar photocatalytic applications. *Appl. Catal. A Gen.* **2018**, *555*, 47–74. [CrossRef]

15. Karthikeyan, C.; Arunachalam, P.; Ramachandran, K.; Al-Mayouf, A.M.; Karuppuchamy, S. Recent advances in semiconductor metal oxides with enhanced methods for solar photocatalytic applications. *J. Alloys Compd.* **2020**, *828*, 154281. [CrossRef]

16. Arunachalam, P.; Amer, M.S.; Ghanem, M.A.; Almayouf, A.M.; Zhao, D. Activation effect of silver nanoparticles on the photoelectrochemical performance of mesoporous TiO$_2$ nanospheres photoanodes for water oxidation reaction. *Int. J. Hydrogen Energy* **2017**, *42*, 11346–11355. [CrossRef]

17. Sakthivel, S.; Neppolian, B.; Shankar, M.V.; Arabindoo, B.; Palanichamy, M.; Murugesan, V. Solar photocatalytic degradation of azo dye: Comparison of photocatalytic efficiency of ZnO and TiO$_2$. *Sol. Energy Mater. Sol. cells* **2003**, *77*, 65–82. [CrossRef]

18. Lu, J.; Hu, H.; Yang, S.; Shanmugam, P.; Wei, W.; Selvaraj, M.; Xie, J. ZnS@carbonaceous aerogel composites fabricated in production of hydrogen and for removal of organic pollutants. *J. Mater. Sci. Mater. Electron.* **2018**, *29*, 8523–8534. [CrossRef]

19. Shi, M.; Wei, W.; Jiang, Z.; Han, H.; Gao, J.; Xie, J. Biomass-derived multifunctional TiO$_2$/carbonaceous aerogel composite as a highly efficient photocatalyst. *RSC Adv.* **2016**, *6*, 25255–25266. [CrossRef]

20. Vadivel, S.; Naveen, A.N.; Theerthagiri, J.; Madhavan, J.; Priya, T.S.; Balasubramanian, N. Solvothermal synthesis of BiPO4 nanorods/MWCNT (1D-1D) composite for photocatalyst and supercapacitor applications. *Ceram. Int.* **2016**, *42*, 14196–14205. [CrossRef]

21. Shanmugam, P.; Murthy, A.P.; Theerthagiri, J.; Wei, W.; Madhavan, J.; Kim, H.-S.; Maiyalagan, T.; Xie, J. Robust bifunctional catalytic activities of N-doped carbon aerogel-nickel composites for electrocatalytic hydrogen evolution and hydrogenation of nitrocompounds. *Int. J. Hydrogen Energy* **2019**, *44*, 13334–13344. [CrossRef]

22. Priya, A.; Senthil, R.A.; Selvi, A.; Arunachalam, P.; Kumar, C.S.; Madhavan, J.; Boddula, R.; Pothu, R.; Al-Mayouf, A.M. A study of photocatalytic and photoelectrochemical activity of as-synthesized WO3/g-C3N4 composite photocatalysts for AO7 degradation. *Mater. Sci. Energy Technol.* **2020**, *3*, 43–50. [CrossRef]

23. Thiagarajan, K.; Bavani, T.; Arunachalam, P.; Lee, S.J.; Theerthagiri, J.; Madhavan, J.; Pollet, B.G.; Choi, M.Y. Nanofiber NiMoO$_4$/g-C$_3$N$_4$ Composite Electrode Materials for Redox Supercapacitor Applications. *Nanomaterials* **2020**, *10*, 392. [CrossRef]

24. Senthil, R.A.; Theerthagiri, J.; Madhavan, J.; Murugan, K.; Arunachalam, P.; Arof, A.K. Enhanced performance of dye-sensitized solar cells based on organic dopant incorporated PVDF-HFP/PEO polymer blend electrolyte with g-C$_3$N$_4$/TiO$_2$ photoanode. *J. Solid State Chem.* **2016**, *242*, 199–206. [CrossRef]

25. Wen, M.Q.; Xiong, T.; Zang, Z.G.; Wei, W.; Tang, X.S.; Dong, F. Synthesis of MoS$_2$/gC$_3$N$_4$ nanocomposites with enhanced visible-light photocatalytic activity for the removal of nitric oxide (NO). *Opt. Express* **2016**, *24*, 10205–10212. [CrossRef]

26. Zhang, X.; Xie, X.; Wang, H.; Zhang, J.; Pan, B.; Xie, Y. Enhanced photoresponsive ultrathin graphitic-phase C3N4 nanosheets for bioimaging. *J. Am. Chem. Soc.* **2013**, *135*, 18–21. [CrossRef]

27. Huang, L.; Li, Y.; Xu, H.; Xu, Y.; Xia, J.; Wang, K.; Xu, Y.; Cheng, X. Synthesis and characterization of CeO$_2$/gC$_3$N$_4$ composites with enhanced visible-light photocatatalytic activity. *RSC Adv.* **2013**, *3*, 22269–22279. [CrossRef]

28. Wang, X.; Maeda, K.; Thomas, A.; Takanabe, K.; Xin, G.; Carlsson, J.M.; Domen, K.; Antonietti, M. A metal-free polymeric photocatalyst for hydrogen production from water under visible light. *Nat. Mater.* **2008**, *8*, 76–80. [CrossRef]

29. Fageria, P.; Nazir, R.; Gangopadhyay, S.; Barshilia, H.C.; Pande, S. Graphitic-carbon nitride support for the synthesis of shape-dependent ZnO and their application in visible light photocatalysts. *RSC Adv.* **2015**, *5*, 80397–80409. [CrossRef]

30. Dong, F.; Wu, L.W.; Sun, Y.J.; Fu, M.; Wu, Z.B.; Lee, S.C. In Situ Construction of g-C3N4/g-C3N4 Metal-Free Heterojunction for Enhanced Visible-Light Photocatalysis. *J. Mater. Chem.* **2011**, *21*, 15171–15174. [CrossRef]

31. Zhang, Y.; Gong, H.; Li, G.; Zeng, H.; Zhong, L.; Liu, K.; Cao, H.; Yan, H. Synthesis of graphitic carbon nitride by heating mixture of urea and thiourea for enhanced photocatalytic H2 production from water under visible light. *Int. J. Hydrogen Energy* **2017**, *42*, 143–151. [CrossRef]

32. Dong, F.; Sun, Y.; Wu, L.; Fu, M.; Wu, Z. Facile transformation of low cost thiourea into nitrogen-rich graphitic carbon nitride nanocatalyst with high visible light photocatalytic performance. *Catal. Sci. Technol.* **2012**, *2*, 1332–1335. [CrossRef]

33. Lu, J.; Zhang, Q.; Wang, J.; Saito, F.; Uchida, M. Synthesis of N-Doped ZnO by grinding and subsequent heating ZnO-urea mixture. *Powder Technol.* **2006**, *162*, 33–37. [CrossRef]

34. Zhang, W.; Zhang, Q.; Dong, F.; Zhao, Z. The Multiple Effects of Precursors on the Properties of Polymeric Carbon Nitride. *Int. J. Photoenergy* **2013**, 685038. [CrossRef]

35. Xiang, Q.; Yu, J.; Jaroniec, M. Preparation and Enhanced Visible-Light Photocatalytic H2-Production Activity of Graphene/C3N4 Composites. *J. Phys. Chem. C* **2011**, *115*, 7355–7363. [CrossRef]

36. Hou, Y.D.; Laursen, A.B.; Zhang, J.S.; Zhang, G.G.; Zhu, Y.S.; Wang, X.C.S. Dahl an I. Chorkendorff. *Angew. Chem. Int. Ed.* **2013**, *52*, 1–6.

37. Yan, H.; Yang, H. TiO2–g-C3N4 composite materials for photocatalytic H2 evolution under visible light irradiation. *J. Alloys Compd.* **2011**, *509*, L26–L29. [CrossRef]

38. Yan, S.C.; Lv, S.B.; Zou, Z.; Li, Z.S. Organic–inorganic composite photocatalyst of g-C3N4 and TaON with improved visible light photocatalytic activities. *Dalton Trans.* **2010**, *39*, 1488–1491. [CrossRef]

39. Sun, J.-X.; Yuan, Y.; Qiu, L.-G.; Jiang, X.; Shena, Y.; Shena, Y.; Zhu, J. Fabrication of composite photocatalyst g-C3N4–ZnO and enhancement of photocatalytic activity under visible light. *Dalton Trans.* **2012**, *41*, 6756–6763. [CrossRef]

40. Wang, Y.; Bai, X.; Pan, C.; He, J.; Zhu, Y. Enhancement of photocatalytic activity of Bi2WO6 hybridized with graphite-like C3N4. *J. Mater. Chem.* **2012**, *22*, 11568–11573. [CrossRef]

41. Cheng, N.; Tian, J.; Liu, Q.; Ge, C.; Qusti, A.H.; Asiri, A.M.; Al-Youbi, A.O.; Sun, X. Au-Nanoparticle-Loaded Graphitic Carbon Nitride Nanosheets: Green Photocatalytic Synthesis and Application toward the Degradation of Organic Pollutants. *ACS Appl. Mater. Interfaces* **2013**, *5*, 6815–6819. [CrossRef]

42. Fu, J.; Chang, B.; Tian, Y.; Xi, F.; Dong, X. Novel C3N4–CdS composite photocatalysts with organic–inorganic heterojunctions: In situ synthesis, exceptional activity, high stability and photocatalytic mechanism. *J. Mater. Chem. A* **2013**, *1*, 3083. [CrossRef]

43. Huang, L.; Xu, H.; Li, Y.; Li, H.; Cheng, X.; Xia, J.; Xu, Y.; Cai, G. Visible-light-induced WO3/gC3N4 composites with enhanced photocatalytic activity. *Dalton Trans.* **2013**, *42*, 8606–8616. [CrossRef]

44. Kuriakose, S.; Choudhary, V.; Satpati, B.; Mohapatra, S. Facile synthesis of Ag–ZnO hybrid nanospindles for highly efficient photocatalytic degradation of methyl orange. *Phys. Chem. Chem. Phys.* **2014**, *16*, 17560–17568. [CrossRef]

45. Kadam, A.; Kim, T.G.; Shin, D.-S.; Garadkar, K.M.; Park, J. Morphological evolution of Cu doped ZnO for enhancement of photocatalytic activity. *J. Alloys Compd.* **2017**, *710*, 102–113. [CrossRef]

46. Barzigari, Z.; Ghazizadeh, A.; Askari, S.Z. Preparation of Mn-doped ZnO nanostructured for photocatalytic degradation of Orange G under solar light. *Res. Chem. Intermed.* **2015**, *42*, 4303–4315. [CrossRef]

47. Kumar, R.; Umar, A.; Rana, D.S.; Sharma, P.; Chauhan, M.; Chauhan, G.S. Fe-doped ZnO nanoellipsoids for enhanced photocatalytic and highly sensitive and selective picric acid sensor. *Mater. Res. Bull.* **2018**, *102*, 282–288. [CrossRef]

48. Kumar, S.; Singh, V.; Tanwar, A. Structural, morphological, optical and photocatalytic properties of Ag-doped ZnO nanoparticles. *J. Mater. Sci. Mater. Electron.* **2015**, *27*, 2166–2173. [CrossRef]

49. Ji, Z.; Luo, Z.; Li, J.; Li, P. Enhanced Photocatalytic Activity of ZnO Toward the Degradation of Methylene Blue Dye: Effects of Fe^{3+} and Sn^{4+} Doping. *Phys. Status Solidi* **2019**, *216*, 1800947. [CrossRef]

50. Raghavan, N.; Thangavel, S.; Venugopal, G. Enhanced photocatalytic degradation of methylene blue by reduced graphene-oxide/titanium dioxide/zinc oxide ternary nanocomposites. *Mater. Sci. Semicond. Process.* **2015**, *30*, 321–329. [CrossRef]

51. Tien, H.N.; Luan, V.H.; Hoa, L.T.; Khoa, N.T.; Hahn, S.H.; Chung, J.S.; Shin, E.W.; Hur, S.H. One-pot synthesis of a reduced graphene oxide–zinc oxide sphere composite and its use as a visible light photocatalyst. *Chem. Eng. J.* **2013**, *229*, 126–133. [CrossRef]

52. Liu, L.; Ma, D.; Zheng, H.; Li, X.; Cheng, M.; Bao, X. Synthesis and characterization of microporous carbon nitride. *Microporous Mesoporous Mater.* **2008**, *110*, 216–222. [CrossRef]

53. Li, X.; Zhang, J.; Shen, L.; Ma, Y.; Lei, W.; Cui, Q.; Zou, G. Preparation and characterization of graphitic carbon nitride through pyrolysis of melamine. *Appl. Phys. A* **2008**, *94*, 387–392. [CrossRef]

54. Le, S.; Jiang, T.; Li, Y.; Zhao, Q.; Li, Y.; Fang, W.; Gong, M. Highly efficient visible-light-driven mesoporous graphitic carbon nitride/ZnO nanocomposite photocatalysts. *Appl. Catal. B Environ.* **2017**, *200*, 601–610. [CrossRef]

55. Isai, K.A.; Shrivastava, V.S. Photocatalytic degradation of methylene blue using ZnO and 2%Fe–ZnO semiconductor nanomaterials synthesized by sol–gel method: A comparative study. *SN Appl. Sci.* **2019**, *1*, 1247. [CrossRef]

56. Mao, Y.; Wu, M.; Li, G.; Dai, P.; Yu, X.; Bai, Z.; Chen, P. Photocatalytic degradation of methylene blue over boron-doped g-C3N4 together with nitrogen-vacancies under visible light irradiation. *React. Kinet. Mech. Catal.* **2018**, *125*, 1179–1190. [CrossRef]

57. Adeleke, J.; Theivasanthi, T.; Thiruppathi, M.; Swaminathan, M.; Akomolafe, T.; Alabi, A. Photocatalytic degradation of methylene blue by ZnO/NiFe2O4 nanoparticles. *Appl. Surf. Sci.* **2018**, *455*, 195–200. [CrossRef]

58. Li, Y.; Wang, K.; Wu, J.; Gu, L.; Lu, Z.; Wang, X.; Cao, X. Synthesis of highly permeable Fe 2 O 3/ZnO hollow spheres for printable photocatalysis. *RSC Adv.* **2015**, *5*, 88277–88286. [CrossRef]

59. Zhu, H.Y.; Jiang, R.; Fu, Y.Q.; Li, R.R.; Yao, J.; Jiang, S.T. Novel multifunctional NiFe2O4/ZnO hybrids for dye removal by adsorption, photocatalysis and magnetic separation. *Appl. Surf. Sci.* **2016**, *369*, 1–10. [CrossRef]

60. Chen, L.; Jiang, D.; He, T.; Wu, Z.; Chen, M. In-situ ion exchange synthesis of hierarchical AgI/BiOI microsphere photocatalyst with enhanced photocatalytic properties. *CrystEngComm* **2013**, *15*, 7556. [CrossRef]

61. Malathi, A.; Arunachalam, P.; Madhavan, J.; Almayouf, A.M.; Ghanem, M.A. Rod-on-flake α-FeOOH/BiOI nanocomposite: Facile synthesis, characterization and enhanced photocatalytic performance. *Colloids Surf. A Physicochem. Eng. Asp.* **2018**, *537*, 435–445. [CrossRef]

62. Fu, H.; Xu, T.; Zhu, S.; Zhu, Y. Photocorrosion Inhibition and Enhancement of Photocatalytic Activity for ZnO via Hybridization with C60. *Environ. Sci. Technol.* **2008**, *42*, 8064–8069. [CrossRef]